Check for updates

OPEN

Iridium Corroles Exhibit Weak Near-Infrared Phosphorescence but Efficiently Sensitize Singlet Oxygen Formation

Ivar K. Thomassen[1], Laura J. McCormick-McPherson[2], Sergey M. Borisov[3]✉ & Abhik Ghosh[1]✉

Six-coordinate iridium(III) triarylcorrole derivatives, Ir[T*p*XPC)]L$_2$, where T*p*XPC = tris(*para*-X-phenyl) corrole (X = CF$_3$, H, Me, and OCH$_3$) and L = pyridine (py), trimethylamine (tma), isoquinoline (isoq), 4-dimethylaminopyridine (dmap), and 4-picolinic acid (4pa), have been examined, with a view to identifying axial ligands most conducive to near-infrared phosphorescence. Disappointingly, the phosphorescence quantum yield invariably turned out to be very low, about 0.02 – 0.04% at ambient temperature, with about a two-fold increase at 77 K. Phosphorescence decay times were found to be around ~5 µs at 295 K and ~10 µs at 77 K. Fortunately, two of the Ir[T*p*CF$_3$PC)]L$_2$ derivatives, which were tested for their ability to sensitize singlet oxygen formation, were found to do so efficiently with quantum yields $\Phi(^1O_2) = 0.71$ and 0.38 for L = py and 4pa, respectively. Iridium corroles thus may hold promise as photosensitizers in photodynamic therapy (PDT). The possibility of varying the axial ligand and of attaching biotargeting groups at the axial positions makes iridium corroles particularly exciting as PDT drug candidates.

The 5d transition metal corroles represent an unusual class of size-mismatched metal-ligand assemblies, which combine a large 5d ion and a sterically constrained, macrocyclic corrole ligand[1]. Although many of the complexes were initially synthesized as part of curiosity-driven exercises, their photophysical properties now promise a wide range of practical applications[2,3], as near-IR emitters, as oxygen sensors, and as photosensitizers for photodynamic therapy, dye-sensitized solar cells, and triplet-triplet annihilation upconversion[4–9]. Iridium corroles were among the first 5d metallocorroles to be synthesized[10] and reported as exhibiting as near-IR phosphorescence at room temperature[4,5]. Subsequently, Au[11–14], OsN[15], ReO[16], and Pt[17] corroles were synthesized and found to exhibit significantly stronger phosphorescence[6–9]. In this reexamination of six-coordinate Ir corroles (structures depicted below), we attempted to determine whether different axial ligands, including pyridine (py), trimethylamine (tma), isoquinoline (isoq), 4-dimethylaminopyridine (dmap), and 4-picolinic acid (4pa), might be exploited to enhance the phosphorescent behavior.

X = CF$_3$, H, F, CH$_3$, OCH$_3$
L = py, tma, isoq, dmap, 4pa
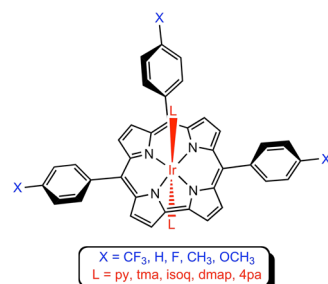
[1]Department of Chemistry, UiT – The Arctic University of Norway, N-9037, Tromsø, Norway. [2]Advanced Light Source, Lawrence Berkeley National Laboratory, Berkeley, California, 94720-8229, United States. [3]Institute of Analytical Chemistry and Food Chemistry, Graz University of Technology, Stremayrgasse 9, 8010, Graz, Austria. ✉e-mail: sergey.borisov@tugraz.at; abhik.ghosh@uit.no
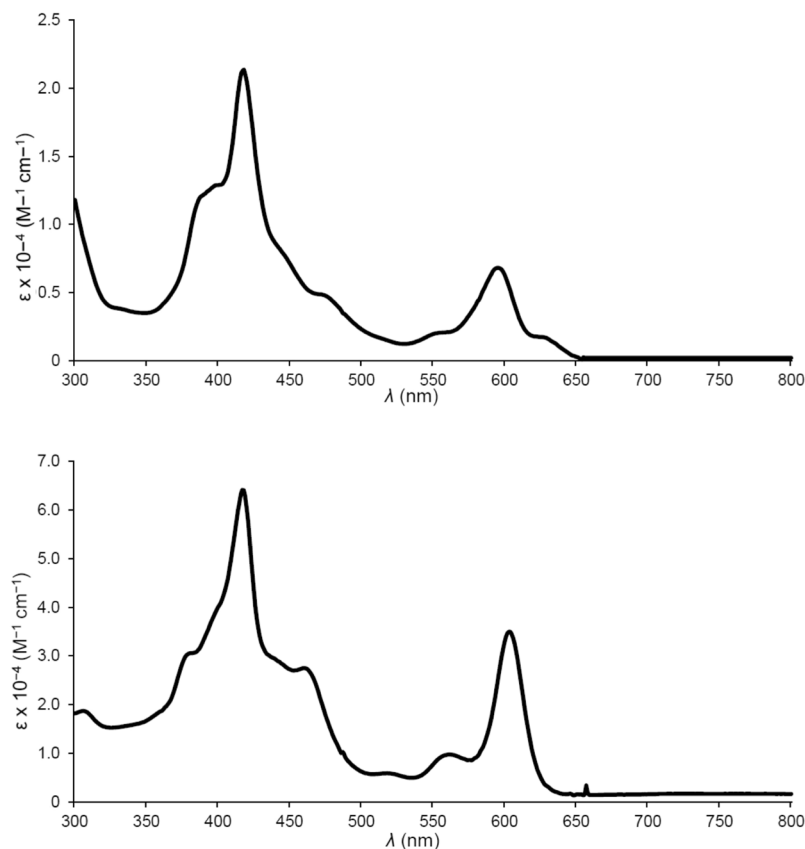
Figure 1. Representative UV-vis spectra in dichloromethane: Ir[(TpMePC)]tma$_2$ (top) and Ir[(TpMePC)]py$_2$ (bottom).

Complex	B	Q	$E_{\frac{1}{2}ox1}$	$E_{\frac{1}{2}ox2}$	$E_{\frac{1}{2}red1}$
Ir[TPC]tma$_2$	384, 416*, 468	596*	0.31	1.09	—
Ir[TPC]py$_2$	414*, 459	562, 602*	0.28	1.00	—
Ir[TpMePC]tma$_2$	384, 417*, 468	598*	0.26	1.02	—
Ir[TpMePC]py$_2$	417*, 460	562, 603*	0.52	1.02	—
Ir[TpOMePC]tma$_2$	384, 417*, 468	600*	0.23	0.94	—
Ir[TpOMePC]py$_2$	416*, 458	563, 605*	0.20	0.89	—
Ir[TpCF$_3$PC]tma$_2$	418*	595*	0.44	1.18	—
Ir[TpCF$_3$PC]py$_2$	416*	602*	0.41	1.11	-1.71
Ir[TpCF$_3$PC]dmap$_2$	418*	606*	—	—	—
Ir[TpCF$_3$PC]4pa$_2$	414*	602*	—	—	—
Ir[TpCF$_3$PC]isoq$_2$	417*	603*	—	—	—

Table 1. Absorption maxima (λ, nm) and redox potentials (V vs. SCE) for Ir(III) corroles in dichloromethane[a]. [a]Asterisks indicate the most intense peaks in the Soret and Q regions.

Results and Discussion

Early spectroscopic and structural studies. Four different *meso*-tris(*para*-X-phenyl)corrole ligands, H$_3$[TpXPC] (X = CF$_3$, H, Me, and OMe), and two different axial ligands, pyridine (py) and trimethylamine (tma), were initially investigated. The compounds were all found to exhibit broad, asymmetric Soret bands with a maximum at 416 ± 2 nm and intense Q bands with the maximum varying over 600 ± 5 nm (Fig. 1 and Table 1). Three of the complexes – Ir[TPC]tma$_2$, Ir[TpMePC]tma$_2$, and Ir[TpCF$_3$PC]py$_2$ (Fig. 2, Table 2) – could be structurally characterized, revealing planar metallocorrole macrocycles with Ir-N$_{corrole}$ distances of 1.95-1.97 Å and Ir-N$_{axial}$ distances of 2.17-2.18 Å. Electrochemical studies revealed two reversible oxidation potentials, including a rather low first oxidation potential that ranged from 0.2 to 0.44 V vs. the saturated calomel electrode (Table 1). In general, a reduction potential could not be observed within the available potential window for the solvent (dichloromethane), except for Ir[TpCF$_3$PC]py$_2$, which showed a reduction potential of -1.71 V, a reflection of the highly electron-rich character of the macrocycle in Ir corroles (Table 1). All these properties are qualitatively consistent with those observed for Ir tris(pentafluorophenyl)corrole derivatives[10].
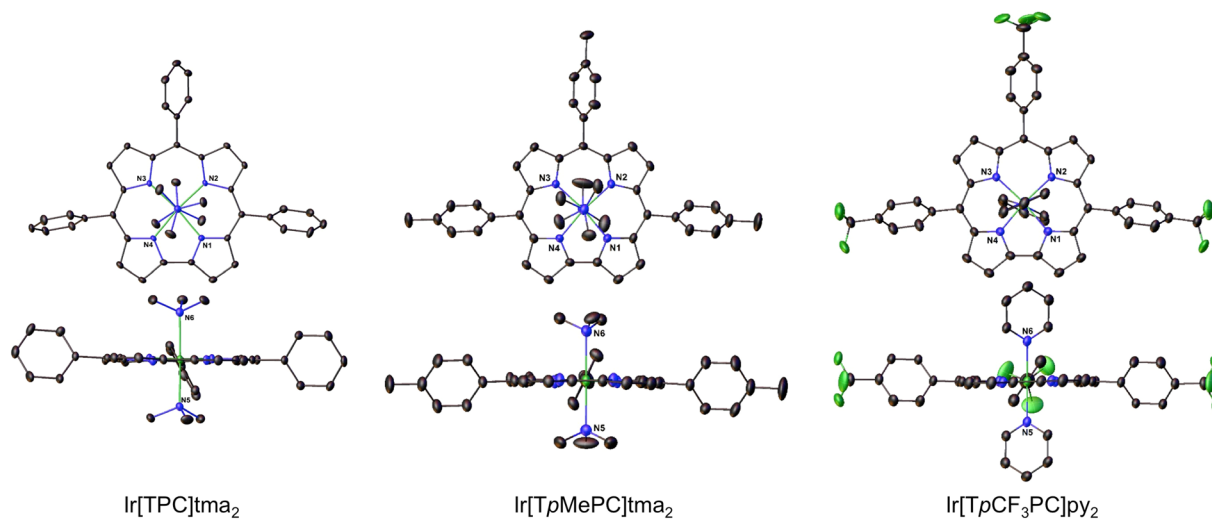
Figure 2. X-ray structures (top and side views) of Ir[TPC]tma$_2$ (left), Ir[TpMePC]tma$_2$ (middle), and Ir[TpCF$_3$PC]py$_2$ (right). Bond distances (Å) for Ir[TPC]tma$_2$: Ir-N1 1.9543(16), Ir-N2 1.9728(16), Ir-N3 1.9745(16), Ir-N4 1.9489(17), Ir-N5 2.1795(18), Ir-N6 2.1672(18). Bond distances (Å) for Ir[TpMePC] tma$_2$. Ir-N1 1.953(2), Ir-N2 1.9746(19), Ir-N3 1.978(2), Ir-N4 1.948(2), Ir-N5 2.178(3), Ir-N6 2.176(3). Bond distances (Å) for Ir[TpCF$_3$PC]py$_2$: Ir-N1 1.946(2), Ir-N2 1.9702(18), Ir-N5 2.055(2); note that N5 and N6 are crystallographically equivalent, as are N2 and N3, and N1 and N4.

Compound	Ir^{III}[TPC]tma$_2$	Ir^{III}[TpMePC]tma$_2$	Ir^{III}[TpCF$_3$PC]py$_2$
Chemical formula	C$_{43}$H$_{41}$IrN$_6$	C$_{54.25}$H$_{66.25}$IrN$_6$	C$_{50}$H$_{30}$F$_9$IrN$_6$
Formula mass	834.02	994.58	1078.00
Crystal system	Monoclinic	Monoclinic	Monoclinic
Space group	$P\,2_1/n$	$P\,2_1/n$	$C\,2/c$
λ [Å]	0.7749	0.7293	0.7749
a [Å]	11.4814(5)	12.8383(7)	18.1543(9)
b [Å]	21.7131(10)	15.3802(8)	16.8434(7)
c [Å]	13.7137(6)	24.6017(13)	14.2251(7)
α [°]	90	90	90
β [°]	94.371(2)	92.934(2)	112.321(2)
Υ [°]	90	90	90
Z	4	4	4
V [Å]	3408.8(3)	4851.4(4)	4023.8(3)
Temperature [K]	100(2)	150(2)	100(2)
Density [g cm^{-3}]	1.625	1.362	1.779
Meas. reflections	46872	91185	40581
Unique reflections	10433	16047	10326
Parameters	457	612	324
Restraints	0	52	6
R_{int}	0.0478	0.0599	0.0431
θ range [°]	1.919-33.659	1.603-32.374	1.867-41.256
R_1, wR_2 all data	0.0276, 0.0551	0.0407, 0.1113	0.0463, 0.0935
S (GooF) all data	1.049	0.828	1.039
Max/min res. dens. [e.Å^{-3}]	1.123/-1.092	0.903/-1.735	3.436/-2.876

Table 2. Crystallographic data for six-coordinate Ir(III) corroles.

Near-IR phosphorescence. For the final set of measurements, we chose to focus on the TpCF$_3$PC derivatives but with an expanded set of axial ligands (L) including py, tma, isoquinoline (isoq), 4-dimethylaminopyridine (dmap), and 4-picolinic acid (4pa). All the complexes were found to exhibit weak phosphorescence in the near-infrared part of the spectrum in anoxic solutions (Fig. 3a). The phosphorescence was almost completely quenched in the presence of molecular oxygen. The excitation spectra (Fig. 3b) matched the absorption spectra very well. As expected, the emission spectra were much narrower at 77 K (Fig. 3c), which enabled more precise determination of the triplet state energies from the edge of the emission spectra. Disappointingly, the
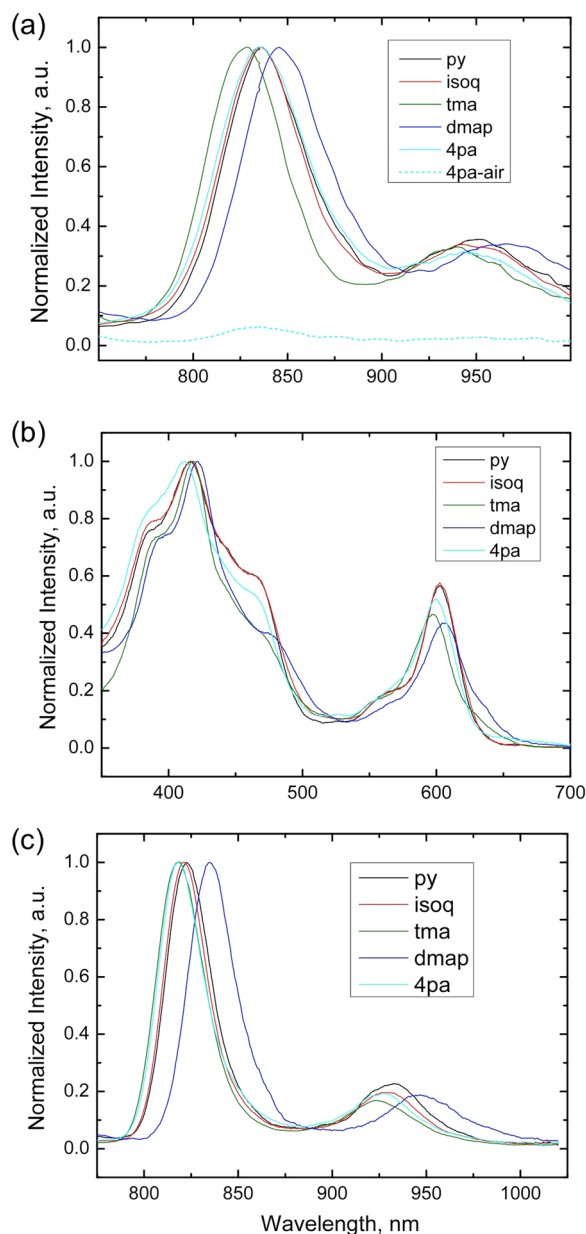
Figure 3. Photophysical properties of Ir-TpCF$_3$PC complexes with the axial ligands indicated. (**a**) Emission spectra in anoxic toluene (unless otherwise mentioned) at 295 K with $\lambda_{ex} = 595$-605 nm (at the maximum of the Q band). The bis-4pa complex was measured in EtOH (anoxic conditions – solid line, air-saturated solvent – dashed line). (**b**) Excitation spectra at 295 K in the same solvents as in (**a**). The emission was detected in the maximum of the emission spectra. RG9 long-pass filter was installed in the emission channel to eliminate the monochromator artefacts. (**c**) Emission spectra in frozen glasses (77 K) with $\lambda_{ex} = 595$-605 nm (at the maximum of the Q-band). The bis-4pa complex was measured in 4:1 v/v ethanol:methanol, while the other complexes were measured in 2:3 v/v toluene:tetrahydrofuran.

phosphorescence quantum yields for all the complexes turned out to be very low, which made their precise estimation difficult. Quantum yields of around 0.02 – 0.04% were estimated at ambient temperature with about a two-fold increase at 77 K. The phosphorescence of the bis-pyridine and bis-isoquinoline complexes was found to be stronger than that of bis-tma and bis-dmap complexes. Furthermore, the emission spectra for the pyridine, isoquinoline, and 4-picolinic acid complexes turned out almost identical (Fig. 3a, Table 3). The decay time profiles for these complexes are mono-exponential (Fig. 4). The fits provide very similar values of ~5 µs at 295 K and ~10 µs at 77 K. Interestingly, in the case of the bis-dmap complex, a relatively long-decaying component was observed both at ambient temperature and at 77 K.

Singlet oxygen sensitization.　Many metalloporphyrins and related compounds are known to be powerful sensitizers of singlet oxygen owing to efficient intersystem crossing and long triplet state lifetimes[3–9]. The fact

Complex	295 K[a]			77K[c]			
	$\lambda_{max,em}$ (nm)	τ (μs)	QY (%)	$\lambda_{max,em}$ (nm)	τ (μs)	QY (%)	E_T^e, cm^{-1}
Ir[TpCF$_3$PC)]py$_2$	836	5.6	~0.04	823	9.8	~0.04	12560
Ir[TpCF$_3$PC]isoq$_2$	836	4.9	~0.04	821	10.4	~0.06	12560
Ir[TpCF$_3$PC]tma$_2$	828	0.6 (38%); 5.1 (62%)	~0.02	818	4.2	~0.06	12630
Ir[TpCF$_3$PC]dmap$_2$	846	2.3 (78%); 8.1 (22%)	~0.02	835	5.2 (61%); 36 (39%)	~0.03	12410
Ir[TpCF$_3$PC]4pa$_2$	836[b]	4.8[b]	~0.02	818[d]	10.7[d]	~0.04	12630

Table 3. Photophysical properties of Ir[TpCF$_3$PC)]L$_2$ derivatives[a–e]. [a]In toluene for all complexes except Ir[TpCF$_3$PC]4pa$_2$. [b]In ethanol. [c]In toluene/tetrahydrofuran (4:6 v/v) for all complexes except Ir[TpCF$_3$PC]4pa$_2$. [d]In ethanol/methanol (4:1 v/v) [e] Estimated from the blue edge of the emission spectrum at 77 K.
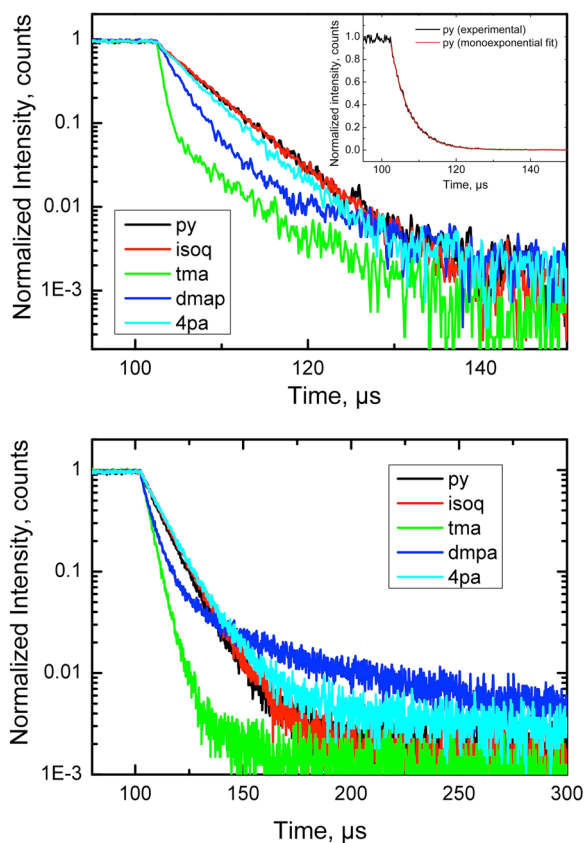
Figure 4. Logarithmic plots for the phosphorescence decay of Ir-TpCF$_3$PC complexes in anoxic solutions at 295 K (above) and in frozen glasses at 77 K (below). The inset depicts the phosphorescence decay of the pyridine complex and the fit according to a monoexponential decay model. The solvents are the same as in Fig. 3.

that Ir corroles exhibit room temperature phosphorescence indicates that the triplet state is populated to at least some degree. In this study, the Ir-TpCF$_3$PC complexes with py and 4pa axial ligands were evaluated for their $^1O_2$ sensitization capabilities. The assay relied on 9,10-dimethylanthracene as a singlet oxygen acceptor[18]. Methylene blue, which exhibits a quantum yield for $^1O_2$ formation [$\Phi(^1O_2)$] of 0.48 and is spectrally compatible with the corroles, was used as the reference[7]. Fig. 5 shows that Ir(III) corroles efficiently sensitize the formation of singlet oxygen. In fact, $\Phi(^1O_2)$ was found to be 0.71 and 0.38 for L = py and 4pa, respectively. The lower value for 4pa correlates with the lower phosphorescence quantum yield for the same complex (Table 3). These $\Phi(^1O_2)$ values are several fold higher than those reported for Ir(III) tris(4-cyanophenyl)corrole derivatives, which might reflect more efficient radiationless deactivation of the triplet states of the latter (which exhibit phosphorescence quantum yields of 0.01%)[5]. Efficient sensitization of $^1O_2$ by Ir(III) complexes is of great interest from the standpoint of photodynamic therapy[19–21] owing to the co-occurrence of two valuable properties: (i) a long excitation wavelength that enables deeper light penetration and (ii) high flexibility in the choice of axial ligands that should facilitate attachment of tumor markers in the axial positions. Covalent attachment via 4-picolinic acid represents a simple, potential synthetic approach for the latter.
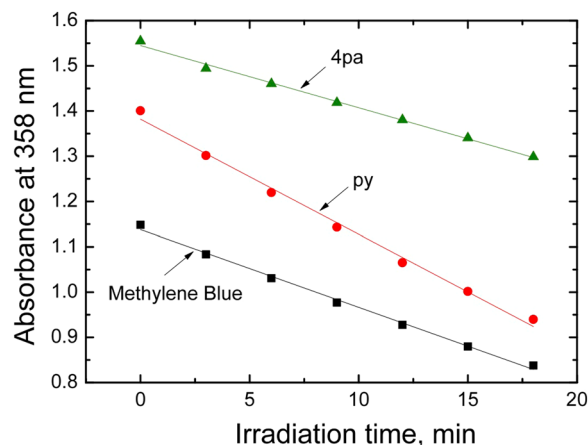
Figure 5. Singlet oxygen-induced degradation of 9,10-dimethylanthracene (c = 0.2 mM) as monitored at 358 nm during photosensitization by two Ir[TpCF$_3$PC)]L$_2$ complexes (L = py and 4pa) and methylene blue in ethanol. Excitation of the sensitizers was performed at 575 nm.

Conclusion

Although the photophysical studies of six-coordinate Ir(III) corroles have been previously reported, only a handful of complexes have been examined to date, all exhibiting weak NIR phosphorescence at room temperature. Several additional complexes were accordingly synthesized and examined herein, with a view to identifying axial ligands most conducive to NIR phosphorescence. Unfortunately, regardless of the triarylcorrole and the axial ligands (which varied over pyridine, trimethylamine, isoquinoline, 4-dimethylaminopyridine, and 4-picolinic acid), the phosphorescence quantum yield turned out to be very low, estimated at around 0.02–0.04% at ambient temperature, with about a two-fold increase at 77 K. Phosphorescence decay times were found to be around ~5 μs at 295 K and ~10 μs at 77 K. Fortunately, two of the Ir[TpCF$_3$PC)]L$_2$ derivatives were found to efficiently sensitize singlet oxygen formation, with quantum yields $\Phi(^1O_2) = 0.71$ and 0.38 for L = py and 4pa, respectively. Iridium corroles thus may hold promise as photosensitizers in photodynamic therapy. The possibility of varying the axial ligand and of attaching tumor-targeting groups at the axial positions makes iridium corroles particularly exciting as drug candidates.

Experimental Section

Materials. Unless otherwise mentioned, all chemicals were obtained from Merck. Silica gel 60 (0.04-0.063 mm particle size, 230-400 mesh) was employed for flash chromatography. Silica gel 60 preparative thin-layer chromatographic plates (20 cm × 20 cm, 0.5 mm thick, Merck) and aluminum oxide 60 preparative thin-layer chromatographic plates (20 cm × 20 cm, 1.5 mm thick, Merck) were used for final purification of all complexes. Free-base corroles were prepared according to previously reported procedures[22,23].

Instrumental methods. The methods used were essentially the same as in our earlier work[11,13,15,16]. UV − visible spectra were recorded on an HP 8453 spectrophotometer. ^{1}H NMR spectra were recorded on a 400 MHz Bruker Avance III HD spectrometer equipped with a 5 mm BB/1H SmartProbe in CDCl$_3$ and referenced to residual CHCl$_3$ 7.26 ppm, C$_6$D$_6$ and referenced to residual C$_6$H$_6$ 7.16 ppm, C$_3$D$_6$O and referenced to residual C$_3$H$_6$O 2.05 ppm or CD$_3$OD and referenced to residual CH$_3$OH 3.31 ppm. High-resolution electrospray-ionization (HR-ESI) mass spectra were recorded from methanolic solution on an LTQ Orbitrap XL spectrometer.

Cyclic voltammetry was performed at 298 K using an EG&G model 263 A potentiostat with a three-electrode system, comprising a glassy carbon working electrode, a platinum wire counter electrode, and a saturated calomel reference electrode (SCE), in CH$_2$Cl$_2$ (distilled from CaH$_2$) as solvent (as in earlier work[11,13,15,16]). The reference electrode was separated from the bulk solution by a fritted-glass bridge filled with the electrolyte solution. The electrolyte solution was purged with argon for several minutes, and electrochemical measurements were conducted under an argon blanket. All potentials are referenced to the SCE.

The phosphorescence of the Ir(III) corroles was studied on a Fluorolog 3 fluorescence spectrometer from Horiba (Japan) equipped with an NIR-sensitive photomultiplier R2658 from Hamamatsu (Japan). The spectra were corrected for the sensitivity of the photomultiplier and smoothing processing (adjusting averaging function) was applied to eliminate noise due to low signals. For measurements at room temperature, dye solutions in a sealable quartz cell (Hellma Analytics, Mülheim, Germany) were deoxygenated by bubbling nitrogen (purity 99.9999%, Linde gas, Austria) for 15 min. Measurements at 77 K were conducted in toluene:tetrahydrofuran (4:6 v/v) or ethanol/methanol (4:1 v/v) frozen glass using accessories for deep-temperature measurements from Horiba. Luminescence decay times were measured on the Fluorolog 3 spectrometer equipped with a DeltaHub module (Horiba Scientific) controlling a SpectraLED-460 light source and using DAS-6 Analysis software for data analysis.

Singlet oxygen generation was studied as previously described[7]. Briefly, a stirred solution containing 9,10-dimethylanthracene (0.2 mM) as a singlet oxygen acceptor and a sensitizer (concentration adjusted to achieve identical absorption for all the sensitizers at λ_{ex}) was irradiated with light from the xenon lamp of the Fluorolog spectrometer (λ_{ex} 575 nm). The degradation of the acceptor was assessed via measurement of the UV-vis spectra.

General procedure for the synthesis of Ir[TpXPC]L$_2$ (X = OMe, CH$_3$, H, CF$_3$, L = tma, py, dmap, 4pa, isoq). The iridium complexes were prepared according to a previously reported procedure[10] with slight modifications. Bis(1,5-cyclooctadiene)diiridium(I) dichloride (Merck, 2 eq) and potassium carbonate (10 eq.) were dissolved in a solution of the free-base corrole (~0.1 mmol, 1 eq) in anhydrous tetrahydrofuran (150 mL). After degassing with argon for a few minutes, the solution was brought to reflux under argon. After 1.5 h, a reagent corresponding to the axial ligand (15 eq) was added all at once and the solution was left to reach room temperature (1 h). For L = tma, the reagent used was trimethylamine *N*-oxide; in the other cases, the unmodifed ligand was used. The reaction mixture was then rotary-evaporated to dryness. Unless otherwise mentioned, the residue was dissolved in a small amount of dichloromethane and subjected to column chromatography (silica, 1:1 CH$_2$Cl$_2$:hexanes) followed by preparative thin-layer chromatography (PTLC, silica, 1:1 CH$_2$Cl$_2$:pentane). Additional details of purification and characterization for each new compound are given below. As in earlier studies of Ir corroles[5,10], accurate elemental analyses could not be consistently obtained; proof of composition and purity was accordingly obtained via thin-layer chromatography, clean high-resolution mass spectra that matched theoretical simulations, and, in three cases, single-crystal X-ray structure determinations.

Ir[TPC]tma$_2$. PTLC afforded the product as a dichroic purple-green solid. Yield 37.5 mg (30%). UV-vis (CH$_2$Cl$_2$) λ_{max} (nm) [ϵ x 10^{-4} (M^{-1}cm^{-1})]: 384 (3.65, sh), 416 (5.58), 468 (1.59, sh), 596 (2.67). ^{1}H NMR (400 MHz, acetone-d_6, δ): 8.88 (d, J = 4.1 Hz, 2H, β-H), 8.62 (d, J = 4.7 Hz, 2H, β-H), 8.39 (d, J = 4.8 Hz, 2H, β-H), 8.24 – 8.19 (m, 4H, 5,15 o-Ph), 8.15 – 8.11 (m, 2H, 10 o-Ph), 8.01 (s, 2H, β-H), 7.78 (dt, J = 14.9, 7.5 Hz, 6H, 5,10,15 m-Ph), 7.69 – 7.63 (m, 3H, 5,10,15 p-Ph), -2.86 (s, 18H, tma-CH$_3$). MS (ESI): M$^+$ = 834.3017 (expt), 834.3019 (calcd for IrC$_{43}$H$_{41}$N$_6$).

Ir[TPC]py$_2$. PTLC afforded the product as a dichroic purple-green solid. Yield 83.4 mg (63.6%). UV-vis (CH$_2$Cl$_2$) λ_{max} (nm) [ϵ x 10^{-4} (M^{-1}cm^{-1})]: 414 (5.30), 459 (2.66, sh), 562 (0.86, sh), 602 (3.37). ^{1}H NMR (400 MHz, acetone-d_6, δ): 8.82 – 8.78 (m, 2H, β-H), 8.62 (dd, J = 4.8, 1.1 Hz, 2H, β-H), 8.38 (d, J = 4.7 Hz, 2H, β-H), 8.28 – 8.22 (m, 4H, 5,15 o-Ph), 8.17 (d, J = 4.1 Hz, 2H, β-H), 8.05 – 8.00 (m, 2H, 10 o-Ph), 7.77 (dd, J = 8.3, 6.8 Hz, 4H, 5,15 m-Ph), 7.70 – 7.59 (m, 5H, 5,15 p-Ph and 10 p,m-Ph), 6.30 (tt, J = 7.6, 1.5 Hz, 2H, p-py), 5.42 – 5.33 (m, 4H, m-py), 1.85 (dt, J = 5.4, 1.5 Hz, 4 H, o-py). MS (ESI): M$^+$ = 874.2403 (expt), 874.2393 (calcd for IrC$_{47}$H$_{33}$N$_6$).

Ir[TpMePC]tma$_2$. PTLC with 1:2 CH$_2$Cl$_2$:pentane afforded the product as a bright green solid. Yield 75.7 mg (49.6%). UV-vis (CH$_2$Cl$_2$) λ_{max} (nm) [ϵ x 10^{-4} (M^{-1}cm^{-1})]: 384 (3.28, sh), 417 (4.88), 468 (1.54, sh), 598 (2.36). ^{1}H NMR (400 MHz, chloroform-d, δ): 8.88 – 8.82 (m, 2H, β-H), 8.66 (d, J = 4.7 Hz, 2H, β-H), 8.39 (d, J = 4.6 Hz, 2H, β-H), 8.03 (dd, J = 47.5, 7.5 Hz, 8H 5,10,15 o-Ph + β-H, 8H), 7.57 (dd, J = 14.0, 7.6 Hz, 6H, 5,10,15 m-Ph), 1.28 (s, 9H, Ph p-CH$_3$), -2.88 (s, 18H, tma-CH$_3$). MS (ESI): M$^+$ = 876.3488 (expt), 876.3489 (calcd for IrC$_{46}$H$_{47}$N$_6$).

Ir[TpMePC]py$_2$. PTLC afforded the product as a dichroic purple-green solid. Yield 36 mg (30.1%). UV-vis (CH$_2$Cl$_2$) λ_{max} (nm) [ϵ × 10^{-4} (M^{-1}cm^{-1})]: 417 (6.40), 460 (2.75, sh), 562 (0.98, sh), 603 (3.49). ^{1}H NMR (400 MHz, benzene-d_6, δ): 9.14 (dd, J = 4.5, 3.0 Hz, 4H, β-H), 8.97 (d, J = 4.8 Hz, 2H, β-H), 8.80 (d, J = 4.2 Hz, 2H, β-H), 8.46 – 8.41 (m, 4H, 5,15 o-Ph), 8.30 (d, J = 7.9 Hz, 2H, 10 o-Ph), 7.42 (d, J = 7.7 Hz, 4H, 5,15 m-Ph), 7.37 (d, J = 8.0 Hz, 2H, 10 m-Ph), 4.79 (t, J = 7.6 Hz, 2H, p-py), 4.17 – 4.11 (m, 4H, m-py), 2.42 (d, J = 4.2 Hz, 9H, Ph -p-CH$_3$), 2.06 (dt, J = 5.3, 1.5 Hz, 4H, o-py). MS (ESI): M$^+$ = 916.2868 (expt), 916.2863 (calcd for IrC$_{50}$H$_{39}$N$_6$).

Ir[TpOMePC]tma$_2$. During initial column chromatography on silica, the eluent was gradually changed from 1:1 CH$_2$Cl$_2$:hexanes to CH$_2$Cl$_2$, and finally to 9:1 CH$_2$Cl$_2$:EtOAc. PTLC with 4:1 EtOAc:CH$_2$Cl$_2$ then afforded the product as a bright green solid. Yield 35.2 mg (29.2%). UV-vis (CH$_2$Cl$_2$) λ_{max} (nm) [ϵ x 10^{-4} (M^{-1}cm^{-1})]: 384 (0.74, sh), 417 (1.05), 468 (0.36, sh), 600 (0.48). ^{1}H NMR (400 MHz, chloroform-d, δ): 8.89 (d, J = 3.8 Hz, 2H, β-H), 8.68 (d, J = 4.7 Hz, 2H, β-H), 8.32 (d, J = 4.6 Hz, 2H, β-H), 8.06 (d, J = 8.0 Hz, 4H, 5,15 o-Ph), 7.92 (d, J = 7.9 Hz, 2H, 10 o-Ph), 7.83 (s, 2H, β-H), 7.33 (dd, J = 11.7, 8.2 Hz, 6H, 5,10,15 m-Ph), 4.09 (d, J = 3.6 Hz, 9H, Ph p-OCH$_3$), -2.86 (s, 18H, tma-CH$_3$). MS (ESI): M$^+$ = 924.3336 (expt), 924.3336 (calcd for IrC$_{46}$H$_{47}$O$_3$N$_6$).

Ir[TpOMePC]py$_2$. PTLC afforded the product as a bright green solid. Yield 31.2 mg (24.5%). UV-vis (CH$_2$Cl$_2$) λ_{max} (nm) [ϵ x 10^{-4} (M^{-1}cm^{-1})]: 416 (3.98), 458 (2.14, sh), 563 (0.77, sh), 605 (2.36). ^{1}H NMR (400 MHz, benzene-d_6, δ): 9.19 – 9.15 (m, 4H, 2 β-H), 8.98 (d, J = 4.9 Hz, 2H, β-H), 8.76 (s, 2H, β-H), 8.42 (d, J = 8.0 Hz, 4H, 5,15 o-Ph), 8.08 (d, J = 8.5 Hz, 2H, 10 o-Ph), 7.20 (d, J = 8.8 Hz, 4H, 5,15 m-Ph), 7.11 – 7.07 (m, 2H, 10 m-Ph), 4.81 (ddd, J = 7.7, 6.2, 1.5 Hz, 2H, p-py), 4.20 – 4.16 (m, 4H, m-py), 3.55 (d, J = 2.0 Hz, 9H, Ph p-OCH$_3$), 2.11 – 2.07 (m, 4H, o-py). MS (ESI): M$^+$ = 964.2738 (expt), 964.2710 (calcd for IrC$_{50}$H$_{39}$O$_3$N$_6$).

Ir[TpCF$_3$PC]tma$_2$. PTLC with 1:3 CH$_2$Cl$_2$:pentane afforded the product as a dark green solid. Yield 14.7 mg (11.8%). UV-vis (CH$_2$Cl$_2$) λ_{max} (nm) [ϵ x 10^{-4} (M^{-1}cm^{-1})]: 418 (2.13), 595 (0.68). ^{1}H NMR (400 MHz, chloroform-d, δ): 8.89 (d, J = 4.2 Hz, 2H, β-H), 8.64 (d, J = 4.8 Hz, 2H, β-H), 8.48 (d, J = 4.8 Hz, 2H, β-H), 8.38 (d, J = 7.8 Hz, 4H, 5,15 o-Ph), 8.29 (d, J = 7.8 Hz, 2H, 10 o-Ph), 8.20 (d, J = 4.2 Hz, 2H, β-H), 8.01 (d, J = 7.9 Hz, 4H, 5,15 m-Ph), 7.98 (d, J = 7.9 Hz, 2H, 10 o-Ph), -2.93 (s, 18H, tma-CH$_3$). MS (ESI): M$^+$ = 1038.2654 (expt), 1038.2641 (calcd for IrC$_{46}$H$_{38}$F$_9$N$_6$).

Ir[T*p*CF₃PC]py₂. PTLC with 1:2 CH₂Cl₂:pentane afforded the product as a dark green solid. Yield 16.3 mg (13.7%). UV-vis (CH₂Cl₂) λ_{max} (nm) [ε x 10⁻⁴ (M⁻¹cm⁻¹)]: 416 (3.86), 602 (1.48). ¹H NMR (400 MHz, benzene-d_6, δ): 9.12 (d, J = 4.3 Hz, 2H, β-H), 8.90 (d, J = 4.8 Hz, 2H, β-H), 8.75 (d, J = 4.8 Hz, 2H, β-H), 8.54 (d, J = 4.3 Hz, 2H, β-H), 8.30 (d, J = 8.0 Hz, 4H, 5,15 o-Ph), 8.23 (d, J = 7.9 Hz, 2H, 10 o-Ph), 7.76 (dd, J = 8.1, 6.6 Hz, 6H, 5,10,15 m-Ph), 4.84 (tt, J = 7.7, 1.5 Hz, 2H, p-py), 4.23 – 4.17 (m, 4H, m-py), 1.86 (dt, J = 5.6, 1.5 Hz, 4H, o-py). MS (ESI): M⁺ = 1078.2032 (expt), 1078.2015 (calcd for IrC₅₀H₃₀F₉N₆).

Ir[T*p*CF₃PC]dmap₂. Initial column chromatography was carried out on neutral alumina with 1:1 CH₂Cl₂:hexanes as eluent. PTLC on alumina with the same eluent afforded the product as a green solid. Yield 31.7 mg (18.1%). UV-vis (CH₂Cl₂) λ_{max} (nm) [ε x 10⁻⁴ (M⁻¹cm⁻¹)]: 418 (1.79), 606 (0.48). ¹H NMR (400 MHz, benzene-d_6, δ): 9.20 (d, J = 4.2 Hz, 2H, β-H), 8.99 (d, J = 4.8 Hz, 2H, β-H), 8.86 (d, J = 4.8 Hz, 2H, β-H), 8.60 (d, J = 4.2 Hz, 2 H, β-H), 8.45 (d, J = 7.9 Hz, 4 H, 5,15 o-Ph), 8.40 (d, J = 7.9 Hz, 2H, 10 o-Ph), 7.77 (dd, J = 8.3, 2.1 Hz, 6H, 5,10,15 m-Ph), 3.57 – 3.52 (m, 4H, m-py), 1.76 – 1.69 (m, 4 H, o-py), 1.07 (s, 6 H, N-CH₃), 1.00 (s, 6H, N-CH₃). MS (ESI): M⁺ = 1164.2855 (expt), 1164.2860 (calcd for IrC₅₄H₄₀F₉N₈).

Ir[T*p*CF₃PC](4pa)₂. Initial column chromatography was carried out on neutral alumina with 1:1 CH₂Cl₂:EtOAc. PTLC on alumina with the same eluent afforded the product as a green solid. Yield 29.6 mg (40.1%). UV-vis (CH₂Cl₂) λ_{max} (nm) [ε x 10⁻⁴ (M⁻¹cm⁻¹)]: 414 (1.71), 602 (0.94). ¹H NMR (400 MHz, methanol-d_4, δ): 8.88 (d, J = 4.2 Hz, 2 H, β-H), 8.61 (d, J = 4.8 Hz, 2 H, β-H), 8.43 – 8.41 (m, 6 H, β-H + 5,15 o-Ph), 8.28 (d, J = 8.0 Hz, 2 H, 10 o-Ph), 8.24 (d, J = 4.3 Hz, 2 H, β-H), 8.08 – 8.03 (m, 4 H, 5,15 m-Ph), 7.99 (d, J = 7.9 Hz, 2 H, 10 m-Ph), 5.61 (d, J = 7.1 Hz, 4 H, m-py), 1.75 (d, J = 7.0 Hz, 4 H, o-py). MS (ESI): M⁻ = 1165.1729 (expt), 1165.1745 (calcd for IrC₅₂H₂₉F₉N₆O₄).

Ir[T*p*CF3PC]isoq₂. Initial column chromatography was carried out on silica with 1:3 CH₂Cl₂:hexanes as eluent. PTLC on silica with the same eluent afforded the product as a green solid. Yield 12.1 mg (7.9%). UV-vis (CH₂Cl₂) λ_{max} (nm) [ε x 10⁻⁴ (M⁻¹cm⁻¹)]: 417 (1.82), 603 (1.02). ¹H NMR (400 MHz, chloroform-d, δ): 8.88 (d, J = 4.2 Hz, 2 H, β-H), 8.69 (d, J = 4.8 Hz, 2 H, β-H), 8.46 (d, J = 4.7 Hz, 2 H, β-H), 8.43 (d, J = 7.9 Hz, 4 H, 5,15 o-Ph), 8.29 (s, 2 H, β-H), 8.24 (d, J = 7.9 Hz, 2 H, 10 o-Ph), 8.05 – 7.99 (m, 4 H, 5,15 m-Ph), 7.93 (d, J = 7.9 Hz, 2 H, 10 m-Ph), 7.07 (ddd, J = 8.2, 6.9, 1.2 Hz, 2 H, isoquinoline C7), 6.93 (ddd, J = 8.2, 6.9, 1.1 Hz, 2 H, isoquinoline C6), 6.76 – 6.72 (m, 2H, isoquinoline C8), 6.40 (d, J = 8.4 Hz, 2 H, isoquinoline C5), 5.58 – 5.54 (m, 2 H, isoquinoline C4), 2.36 (s, 2 H, isoquinoline C1), 1.68 (d, J = 6.9 Hz, 2 H, isoquinoline C3). MS (ESI): M⁻ = 1178.2351 (expt), 1178.2329 (calcd for IrC₅₈H₃₄F₉N₆).

X-ray structure determinations. X-ray data for Ir[TPC]tma₂, Ir[T*p*MePC]tma₂, and Ir[T*p*CF₃PC] py₂ were collected on beamline 11.3.1 at the Advanced Light Source, Lawrence Berkeley National Laboratory. Samples were mounted on MiTeGen kapton loops and placed in a 100(2)-K (for Ir[TPC]tma₂ and Ir[T*p*CF₃PC] py₂) or 150(2)-K (for Ir[T*p*CF₃PC]py₂) nitrogen cold stream provided by an Oxford Cryostream 800 Plus low-temperature apparatus on the goniometer head of a Bruker D8 diffractometer equipped with a PHOTON100 CMOS detector operating in shutterless mode. Diffraction data were collected using synchrotron radiation monochromated using silicon(111) to a wavelength of 0.7293(1)Å (for Ir[T*p*MePC]tma₂) or 0.7749(1)Å (for Ir[TPC] tma₂ and Ir[T*p*CF₃PC]py₂). An approximate full-sphere of data was collected using a combination of φ and ω scans with scan speeds of one second per degree for the φ scans and one and three seconds per degree for the ω scans at 2θ = 0° and −45°, respectively. The structures were solved by intrinsic phasing (SHELXT[24]) and refined by full-matrix least-squares on F^2 (SHELXL-2014[25]). All non-hydrogen atoms were refined anisotropically. Hydrogen atoms were geometrically calculated and refined as riding atoms. Additional crystallographic information has been summarized in Table 2.

References

1. Ghosh, A. Electronic Structure of Corrole Derivatives: Insights from Molecular Structures, Spectroscopy, Electrochemistry, and Quantum Chemical Calculations. *Chem. Rev.* **117**, 3798–3881 (2017).
2. Teo, R. D., Hwang, J. Y., Termini, J., Gross, Z. & Gray, H. B. Fighting Cancer with Corroles. *Chem. Rev.* **117**, 2711–2729 (2017).
3. Mahammed, A. & Gross, Z. Corroles as triplet photosensitizers. *Coord. Chem. Rev.* **379**, 121–132 (2019).
4. Palmer, J. H., Durrell, A. C., Gross, Z., Winkler, J. R. & Gray, H. B. Near-IR Phosphorescence of Iridium(III) Corroles at Ambient Temperature. *J. Am. Chem. Soc.* **132**, 9230–9231 (2010).
5. Sinha, W., Ravotto, L., Ceroni, P. & Kar, S. NIR-Emissive Iridium(III) Corrole Complexes as Efficient Singlet Oxygen Sensitizers. *Dalton Trans.* **44**, 17767–17773 (2015).
6. Alemayehu, A. B. *et al.* Gold Tris(carboxyphenyl)corroles as Multifunctional Materials: Room Temperature Near-IR Phosphorescence and Applications to Photodynamic Therapy and Dye-Sensitized Solar Cells. *ACS Appl. Mater. Interfaces* **8**, 18935–18942 (2016).
7. Borisov, S. M., Alemayehu, A. & Ghosh, A. Osmium-Nitrido Corroles as NIR Indicators for Oxygen Sensors and Triplet Sensitizers for Organic Upconversion and Singlet Oxygen Generation. *J. Mater. Chem. C* **4**, 5822–5828 (2016).
8. Lemon, C. M., Powers, D. C., Brothers, P. J. & Nocera, D. G. Gold Corroles as Near-IR Phosphors for Oxygen Sensing. *Inorg. Chem.* **56**, 10991–10997 (2017).
9. Alemayehu, A. B., McCormick, L. J., Gagnon, K. J., Borisov, S. M. & Ghosh, A. *ACS Omega* **3**, 9360–9368 (2018).
10. Palmer, J. H. *et al.* Iridium Corroles. *J. Am. Chem. Soc.* **130**, 7786–7787 (2008).
11. Alemayehu, A. B. & Ghosh, A. Gold Corroles. *J. Porphyrins Phthalocyanines* **15**, 106–110 (2011).
12. Rabinovitch, E., Goldberg, I. & Gross, Z. Gold(I) and Gold(III) Corroles. *Chem. Eur. J* **17**, 12294–12301 (2011).
13. Thomas, K. E., Alemayehu, A. B., Conradie, J., Beavers, C. & Ghosh, A. Synthesis and Molecular Structure of Gold Triarylcorroles. *Inorg. Chem.* **50**, 12844–12851 (2011).

14. Thomas, K. E. *et al*. Ligand Noninnocence in Coinage Metal Corroles: A Silver Knife-Edge. *Chem. Eur. J* **21**, 16839–16847 (2015).
15. Alemayehu, A. B., Gagnon, K. J., Terner, J. & Ghosh, A. Oxidative Metalation as a Route to Size-Mismatched Macrocyclic Complexes: Osmium Corroles. *Angew. Chem. Int. Ed* **53**, 14411–14414 (2014).
16. Einrem, R. F., Gagnon, K. J., Alemayehu, A. B. & Ghosh, A. Metal-Ligand Misfits: Facile Access to Rhenium-Oxo Corroles by Oxidative Metalation. *Chem. Eur. J* **22**, 517–520 (2016).
17. Alemayehu, A. B. *et al*. Platinum Corroles. *Chem. Comm* **50**, 11093–11096 (2014).
18. Gross, E., Ehrenberg, B. & Johnson, F. M. Singlet Oxygen Generation by Porphyrins and the Kinetics of 9,10-Dimethylanthracene Photosensitization in Liposomes. *Photochem. Photobiol.* **57**, 808–813 (1993).
19. Bonnett, R. Chemical Aspects of Photodynamic Therapy. 1-324 (CRC, 2000).
20. Pandey, R. K., Kessel, D. & Dougherty, T. J. (eds.) *Handbook of photodynamic therapy: updates on recent applications of porphyrin-based compounds*. 1–564 (World Scientific, 2016).
21. Nardis, S., Mandoj, F., Stefanelli, M. & Paolesse, R. Metal complexes of corrole. *Coord. Chem. Rev.* **388**, 360–405 (2019).
22. Gryko, D. T. & Koszarna, B. Refined methods for the synthesis of *meso*-substituted A$_3$- and trans-A$_2$B-corroles. *Org. Biomol. Chem.* **1**, 350–357 (2003).
23. Koszarna, B. & Gryko, D. T. Efficient Synthesis of *meso*-Substituted Corroles in a H$_2$O − MeOH Mixture. *J. Org. Chem.* **71**, 3707–3717 (2006).
24. Sheldrick, G. M. SHELXT - Integrated Space-Group and Crystal-Structure Determination. *Acta Cryst* **A71**, 3–8 (2015).
25. Sheldrick, G. M. Crystal Structure Refinement with SHELXL. *Acta Cryst* **C71**, 3–8 (2015).

Acknowledgements

Author contributions

I.K.T. carried out all chemical syntheses, L.M.M. did the X-ray structure determinations, and S.M.B. did the photophysical studies. A.G. planned and coordinated the research. All authors contributed to writing the manuscript text.

Competing interests

The authors declare no competing interests.

Additional information

Supplementary information is available for this paper at https://doi.org/10.1038/s41598-020-64389-3.

Correspondence and requests for materials should be addressed to S.M.B. or A.G.

Reprints and permissions information is available at www.nature.com/reprints.

Publisher's note Springer Nature remains neutral with regard to jurisdictional claims in published maps and institutional affiliations.